JOURNAL OF APPLIED ELECTROCHEMISTRY 25 (1995) 1113–1121

Electrodeposition of nickel/silicon carbide composite coatings on a rotating disc electrode

G. MAURIN, A. LAVANANT

Laboratoire Physique des Liquides et Electrochimie, UPR15 du CNRS associé à l'Université P. & M. Curie, Tour 22, 4 Place Jussieu, 75252 Paris Cedex 05, France

Received 14 December 1994; revised 20 February 1995

Composite coatings suitable for protection against wear were prepared by electrodeposition from a nickel Watts solution containing silicon carbide particles maintained in suspension. To obtain a better understanding of hydrodynamic effects on the codeposition process a rotating disc electrode, immersed in a vertical rising flow, was used. The local concentration of embedded SiC along the radius of the disc electrode was studied as a function of suspension concentration, rotation rate and the particle mean diameter. The effect of a rheoactive polymer was also examined. Although it is generally admitted that the particle incorporation rate is governed by a two-step adsorption process, the experimental results show that it is also dependent on the spatial distribution of the wall fluid flow. The normal component of the fluid velocity promotes particle impingement, whereas the parallel component tends to eject the loosely fixed particles. The competition between the forces which tend to maintain particles attached to the surface and the shear force which tends to remove them, depends on several parameters, in particular the surface chemistry and the size of the particles, the flow rate and the current density.

List of symbols

A, B	Tafel coefficients according to metal and particle deposition, respectively
α_v	volume ratio of the amount of codeposited particles (vol %)
α_w	weight ratio of the amount of codeposited particles (vol %)
C	concentration of the particles in suspension in the bath (g dm^{-3})
F_{adh}, F_{stagn}, F_{shear}, F_{fric}	forces exerted on particles (adhesion, stagnation, ejection, friction)
η	overpotential (V)
i	current density (A dm^{-2})
K	Langmuir coefficient (g^{-1} dm^3)
T	constant coefficient in Equation 2
V_r, V_z	radial and normal component of the fluid velocity (cm s^{-1})
Ω	rotation rate of the disc electrode (rpm)
Ω_c	critical rotation rate (rpm)

1. Introduction

Composite coatings can be prepared by electrodeposition from an electrolytic solution containing a suspension of insoluble particles [1]. Interesting applications have been developed for purposes of wear resistance [2, 3], dry lubrication [4, 5], anticorrosion [6, 7] and dispersion hardening [8, 9].

Many systems were studied, including metals such as copper [10–13, 32], nickel [2, 3, 8, 9, 14], silver [5], cobalt [15, 16], lead [17] and gold [18, 35]. A great variety of particles was also used, including inert materials such as diamond [19], ceramic materials such as silicon carbide [2, 5, 20–23], titanium carbide [17], chromium carbide [6], alumina [8 to 11, 25], titania [9, 20], chromium oxide [16], lubricant materials such as PTFE [26], graphite [27] or molybdenium sulfide [4, 5] and also metallic materials such as chromium [28, 29]. Because of their excellent tribological properties nickel/silicon carbide coatings were first developed to protect the NSU-Wankel rotary engine [23] against wear and are used as substitutes for hard chromium coatings in four-stroke or two-stroke aluminium engines [3, 31].

According to the literature, the rate of particle entrapment depends on many factors either related to the particles (size, density, composition, zeta potential [11, 25, 30, 39], conductivity [40]) or to the electrolytic solution (composition, pH, temperature, presence of additives [21, 30, 32]). Agitation of the bath appears to be an important factor but its effects are somewhat ambiguous. In most cases particle sizes are larger than 0.1 μm and therefore vigorous stirring of the electrolyte is necessary to obtain a homogeneous suspension. Various stirring techniques have been employed [1, 16]. In some industrial

0021-891X

processes, several of these techniques are employed simultaneously [15, 26]. However, it has sometimes been observed that increase in fluid velocity results in a decrease in the incorporation rate of solid particles [30, 33].

The cause of the incorporation of inert particles into the deposit has been attributed to a simple mechanical entrapment [34] or to electrophoretic forces acting on the electrically charged particles [25]. In 1972, Guglielmi proposed a simple two-step model [20]. The particles are assumed to be covered by adsorbed metal ions M^{2+}_{ads}. In the first step, particles are loosely adsorbed at the cathodic interface. The surface coverage, σ, is expressed by a slightly modified Langmuir adsorption isotherm:

$$\sigma = \frac{KC}{1+KC}(1-\Theta) \qquad (1)$$

where K is the adsorption coefficient, C the concentration of the particles in the electrolyte and Θ the surface coverage by particles which are still definitively attached to the coating. Effectively, in many experimental investigations α_v tends to an asymptotic limit for increasing values of suspension concentration. During the second step, the loosely adsorbed particles are definitively attached to the deposit by the electrolytic reduction of the adsorbed ions M^{2+}_{ads}. By assuming, that both M^{2+} and M^{2+}_{ads} reduction rates obey Tafel laws the following equation was derived:

$$\frac{C}{\alpha_v} = Te^{(B-A)\eta}\left(\frac{1}{K}+C\right) \qquad (2)$$

where the symbols are explained at the start of this paper.

According to Equation 2, plots of C/α_v against C for various constant overpotentials (or current densities) are straight lines converging at a common point $C_0 = -1/K$ on the C axis. Guglielmi obtained experimental results which were in good agreement with his own predictions. In particular he observed that α_v was an increasing function of i in the case of Ni/SiC codeposition, whereas it was a decreasing function in the case of Ni/TiO_2 codeposition [20].

It is important to note that hydrodynamics does not play any role in this model. Furthermore, the Tafel relation used in Equation 2 is valid only in the case of a reaction rate limitation and can not be used when the current density or the particle flow is limited by mass transport.

Celis *et al.* [11, 18, 30, 35–37] studied the codeposition of copper or gold with alumina on a rotating disc electrode and derived a mathematical model where it was assumed that free and adsorbed metallic ions are equal with respect to transport and to reduction processes and that a particle would be attached to the metal if a given amount of adsorbed ions was reduced during its residence time in the vicinity of the cathodic interface [36, 37]. α_v increases with current density as long as the deposition rate is under charge transfer control and decreases when the current is limited by mass transport of ionic species. It was also experimentally observed that electrolyte stirring modifies the α_v against i relationship even for metals for which the deposition rate is not limited by mass transport of ionic species. For example, in the Ni/SiC system, Kariapper and Foster [38] observed than an increase in the bath agitation can completely reverse the relationship between α_v and the current density.

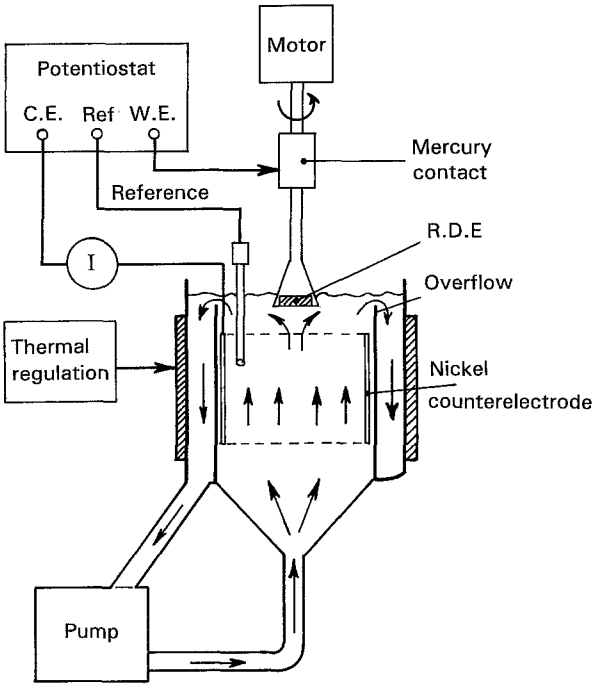

Fig. 1. Scheme of the experimental setup used for the electrodeposition of composite coatings.

The aim of the present study is to obtain a better understanding of the effects of fluid flow on the incorporation rate of inert particles with the electrodeposited metal. Nickel/SiC composite coatings were deposited onto a rotating disc electrode which has the advantage of uniform accessibility to mass transport. The radial distribution of the local volume fraction of embedded particles was studied as a function of the rotation rate, the particle concentration, the particle size and the current density. The hydrodynamic conditions were also modified by adding a rheoactive polymer to the electrolyte.

2. Experimental details

2.1. *Experimental setup*

The plating cell was a cylindrical glass vessel with a conical bottom (Fig. 1). The electrolyte, which contained SiC powder in suspension, ascended from the bottom of the cell and spilled over the rim into a concentric compartment; it was recirculated by means of a centrifugal pump. The pumping rate was adjusted to ensure a very slow ascension velocity of the particle suspension, just sufficient to avoid sedimentation. Working electrodes were 12 to 20 mm diameter discs immersed in the stagnation region of the ascending flow. They were made of polished titanium or nickel.

Table 1. Main characteristics of the various silicon carbide powders used for the preparation of the composite coatings plating baths

SiC powder	*Mean diameter* /μm	*BET area* /$m^2 g^{-1}$	*Main bulk impurities* /wt %	*Surface composition*	*Crystal structure*
Lonza					
UF 05	2.8	4.57	Fe 0.95%	SiO	α(III) and β
UF 10	1.8	10	P 0.7%		
UF 15	0.8	15.6			
UF 32	0.1	≈ 32			
Wolters	4	2.55	N 0.13% Fe 0.5%	SiC + ϵ SiO	α(III) + α(II)
Ibidens	10	0.9	Total < 1%	SiO + SiC	β

By using a ferri/ferro-cyanide redox couple, and by measuring the limiting current, it was verified that in the vicinity of the electrode, the fluid flow is governed by the disc rotation and not by electrolyte recirculation at rotation speed > 200 rpm.

For nickel electrodeposition the plating solution was a Watts bath ($NiSO_4.7H_2O$ 300 g dm^{-3}; $NiCl_2$ 30 g dm^{-3}; H_3BO_3 40 g dm^{-3}). The pH was adjusted to 4.5 and the temperature was maintained at (50.0 ± 0.5) °C. In a limited number of experiments, small quantities of xanthan gum, which is a long chain rheoactive polymer, were added to the electrolyte to test its effect on particle incorporation. Electrodeposition was performed potentiostatically or galvanostatically. Electrode potential was measured against a saturated calomel reference electrode (SCE). A large pure nickel sheet was used as soluble anode.

2.2. *SiC powder characterization*

Silicon carbide powders from various manufacturers (Lonza, Wolters and Ibiden) were used. Particle sizes were measured by means of a Sedigraph apparatus and morphology was observed by scanning electron microscopy. SiC composition was analysed by atomic absorption and surface concentration profiles were determined by SIMS. The crystal structure of SiC is generally a mixture of several cubic and hexagonal phases which were identified by X-ray powder diffraction. The main data are summarized in Table 1. It is worth noting that the superficial layer of the Lonza silicon carbide contains a much greater quantity of oxygen than of the other SiC powders.

According to SEM observation, Lonza and Wolters particles exhibited very irregular shapes and often appeared like platelets with sharp edges resulting from cleavage along dense lattice planes during the grinding of the bulk material. Conversely, Ibiden-S particles, which were prepared by a different technique, were more or less round shaped. Most experiments presented in this paper were carried out with Lonza SiC powders because five grains sizes of the same material quality were available.

2.3. *Composite coating analysis*

Composite coatings were separated from their titanium substrate; they were calcined and the resulting CO_2 was determined by infrared absorption spectroscopy. By using this method, the mean concentration of embedded SiC was evaluated. The measurement error on the mean SiC percentage is about ±0.2%.

The local SiC concentration, α_L, was evaluated by EDX analysis by measuring the ratio between the intensities of a silicon peak and a nickel peak, and by comparing with a homogeneous standard. To determine the radial distribution α_L against r of incorporated SiC in a disc electrode, several sets of measurements were performed every few millimetres along a radius of the disc. The domain of analysis was a 100 μm × 100 μm square, small enough to characterize the local concentration but sufficiently large to obtain reasonable precision (±0.5%).

3. Results

3.1. *Mean fraction of incorporated SiC*

Figure 2 shows the mean weight fraction, α_w, of silicon carbide incorporated in 50 μm thick composite layers deposited on a 12 mm electrode against the

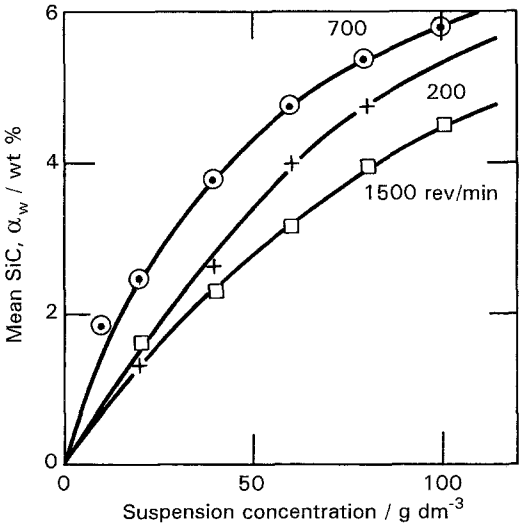

Fig. 2. Mean weight concentration α_w of incorporated SiC within nickel electrocoating against UF 05 SiC concentration in the bath for various rotations velocities (i = 5 A dm^{-2}, electrode diameter: 12 mm).

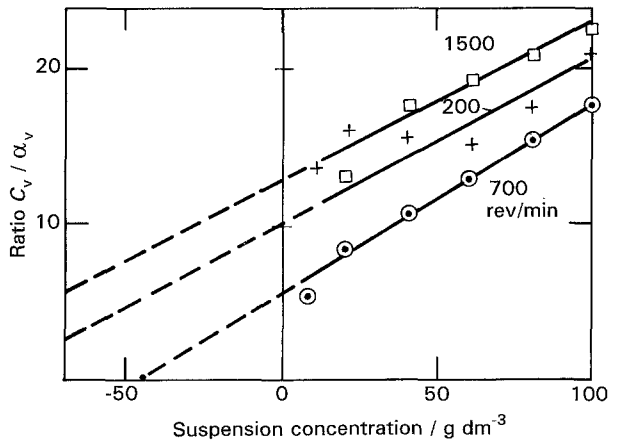

Fig. 3. Same experimental results as for Fig. 2 plotted in a C/α_v against C Guglielmi coordinates system.

UF 05 powder concentration in the plating bath, for a constant current density (5 A dm^{-2}) and for several rotation velocities. The results are apparently in good agreement with the Guglielmi model. Effectively, α_w against C curves have the general shape of an adsorption isotherm; the asymptotic value of α_w is approximately 10% by weight (or $\sim$ 25% by volume). The same experimental results were also plotted as C/α against C as proposed by Guglielmi (Fig. 3). The curves are straight lines in agreement with Equation 2. The adsorption coefficients, K, deduced from these curves are given in Table 2. These data clearly show that the first step in the codeposition process is strongly dependent on fluid flow. K varies with rotation velocity and the relationship is not monotonic; the highest values are obtained for intermediate velocities. This appears to contradict the fact that an adsorption coefficient is normally expected to be independent of the system hydrodynamics.

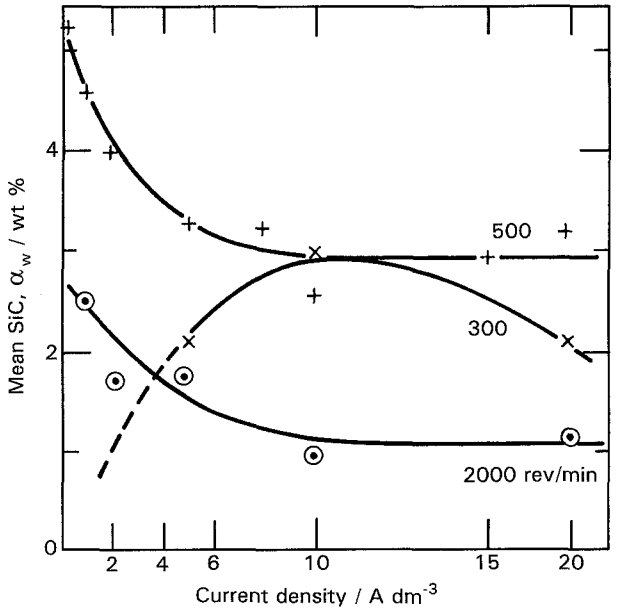

Fig. 4. Mean weight concentration of incorporated UF 05 SiC against current density for three rotation velocities (particle concentration $C = 20$ g dm^{-3}, electrode diameter: 12 mm)

Table 2. Adsorption coefficients K for various rotation velocities deduced from Fig. 3 according to the Guglirlmi model. (UF 05 SiC: $i = 5$ A dm^{-2})

Ω/rpm	200	700	1500
$K/10^{-3}$ g^{-1} dm^3	10.6	22.2	7.9

To examine the influence of fluid flow on the second step of the codeposition process, α_w was measured and plotted against current density between 0.5 and 20 A dm^{-2} for a constant suspension concentration ($C = 20$ g dm^{-3}; UF 05) and for several rotation rates. When Ω is greater than 400 rpm, α_w is a monotonic and decreasing function of the current. On a log/log plot the curve is a straight line with a negative slope, the value of which depends on the rotation velocity. When Ω is less than 400 rpm, α_w becomes small, increases with i, passes through a maximum and finally decreases for higher current intensities (Fig. 4). In the same way, the ratio B/A deduced from Equation 2 can be lower or larger than 1 depending on the rotation rate.

Another effect of rotation rate is illustrated by Fig. 5 where the mean weight fraction is plotted against Ω for a constant current density, for two electrode diameters and for two suspension concentrations. Two regimes are evident: at low rotation velocities, increase in Ω has a beneficial effect on the particle incorporation. This can be attributed to the larger convective flow towards the disc electrode. Conversely, at high rotation velocity, the incorporation tends to decrease with Ω. In this last case, the intense radial flow ejects loosely attached particles. Figure 5 also illustrates the dependence of α_w on the electrode radius. At high rotation rate, the mean incorporated weight fraction is lower for a 20 mm disc than for a 12 mm one, although the suspension concentration was 40 g dm^{-3} in the first case and only 20 g dm^{-3} in the

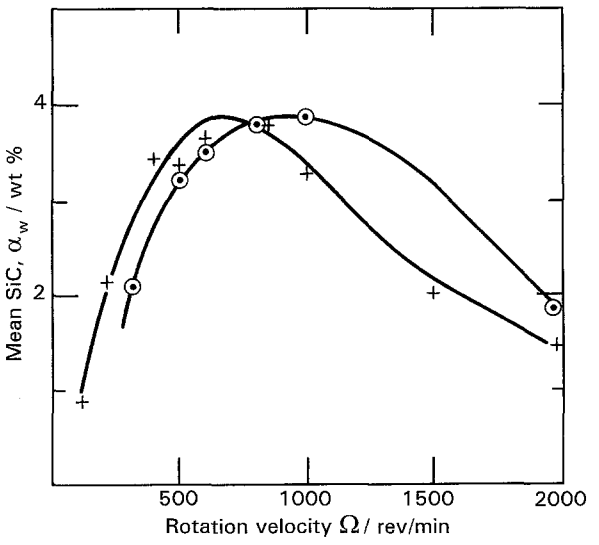

Fig. 5. Mean weight concentration of incorporated UF 05 SiC against rotation velocity ($i = 5$ A dm^{-2}). (○): $C = 20$ g dm^{-3}; electrode diam: 12 mm; (+): $C = 40$ g dm^{-3}; electrode diam: 20 mm.

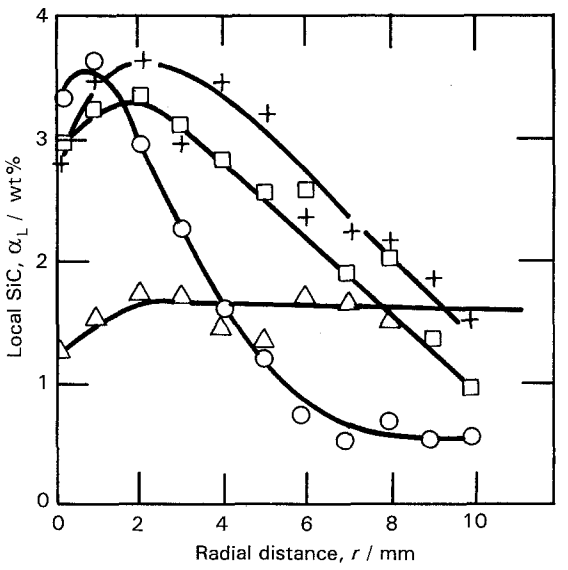

Fig. 6. Radial distribution of the local concentration α_L of UF 10 SiC in a 20 mm disc electrode for various rotation velocities: (△) 300 rpm, (+) 500 rpm, (□) 700 rpm and (○) 1500 rpm.

second. This supports the hypothesis of an ejection effect, the importance of which increases with the wall fluid velocity and, therefore, with the radial distance.

3.2. *Local fraction of incorporated SiC*

The local concentration α_L was measured along a disc radius for composite coatings prepared over a large range of experimental conditions [42, 43]. The influence of rotation velocity, Ω, is illustrated in Fig. 6. Two regimes occur: in the *low velocity regime*, the local concentration is weak and practically constant over the entire electrode. In the *high velocity regime*, above a critical velocity ($\Omega_c = 400$ rpm in the present case), the local concentration measured at the centre is much larger and is nearly independent of Ω. However, away from the centre, α_L decreases as the radial distance r increases. This effect increases with the rotation rate. For example, at 1500 rpm, α_L is three times lower near the electrode rim than in the centre. This explains why, in the previous results, the mean concentration was lower on a large disc than on a small one (Fig. 5). In some cases, near the centre, a small secondary minimum was observed; this was probably due to slight eccentricity of the rotation.

The radial distribution of SiC content results not only from a reduction in the number of entrapped particles at increasing radial distances but also from the decrease of the particle size. At long radial distances, only very small particles are detected by SEM. It can therefore be concluded that the biggest particles are preferentially ejected by the radial component of the fluid flow. It was also observed that, in most cases, the emerging SiC platelets are not fixed to the nickel along their large flat cleavage faces but stand vertically. This phenomenon is probably due to the anisotropic properties of SiC crystals.

The radial distribution of incorporated SiC also depends on the concentration of the particle suspension. Two sets of curves are presented in Fig. 7. They correspond to two values of C and to two rotation rates. In the low velocity regime, α_L is practically independent of r, but increases with C. In the high velocity regime, α_L is practically constant near the disc centre, whereas it decreases with r more slowly for a larger concentration, C. The Guglielmi assumption of a saturation of the incorporation rate is confirmed in the central region of the electrode. Moreover, for $\Omega > \Omega_c$, it appears that the suspension concentration on one hand, the electrode radius and the rotation velocity on the other, have opposite effects on the codeposition rate. This is illustrated by

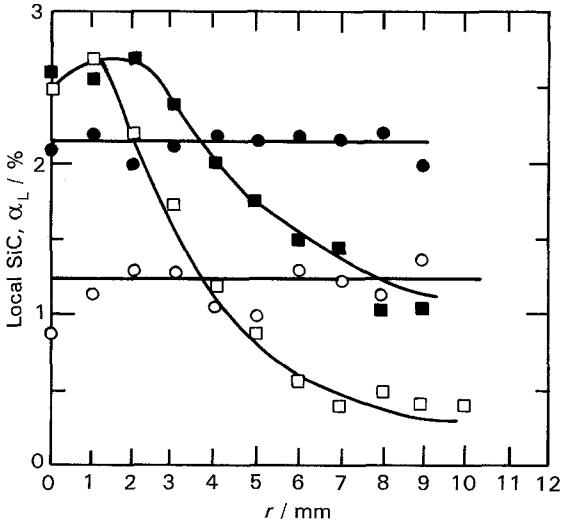

Fig. 7. Radial distribution of the local concentration α_L of UF 10 SiC for two particle concentrations and two rotation velocities. ($i = 10$ A dm^{-2}). $C = 40$ g dm^{-3}: (●) 300 rpm and (■) 1500 rpm; $C = 20$ g dm^{-3}: (○) 300 rpm and (□) 1500 rpm.

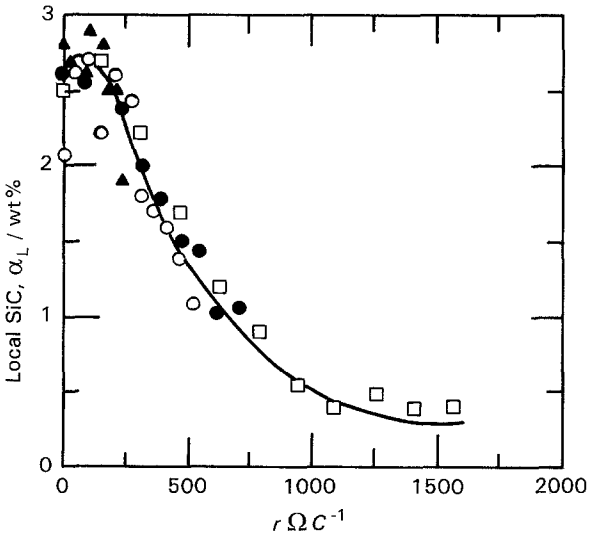

Fig. 8. Local concentration of UK 10 SiC against the reduced variable ($r\Omega C^{-1}$) for particle two concentrations and two rotation velocities. $C = 40$ g dm^{-3}: (○) 500 rpm and (□) 1500 rpm; $C = 20$ g dm^{-3}: (△) 500 rpm and (■) 1500 rpm.

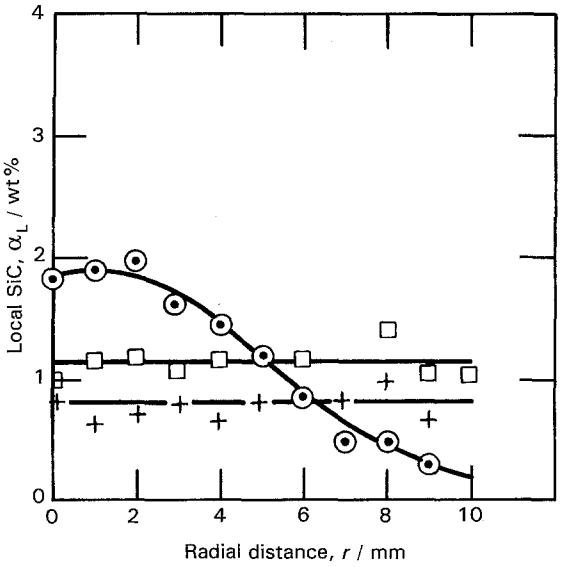

Fig. 9. Radial distribution of the local concentration α_L of UF 15 SiC in a 20 mm disc electrode for various rotation velocities. ($C = 20\,g\,dm^{-3}$; $i = 5\,A\,dm^{-2}$). (+) 500 rpm, (□) 700 rpm and (○) 1500 rpm.

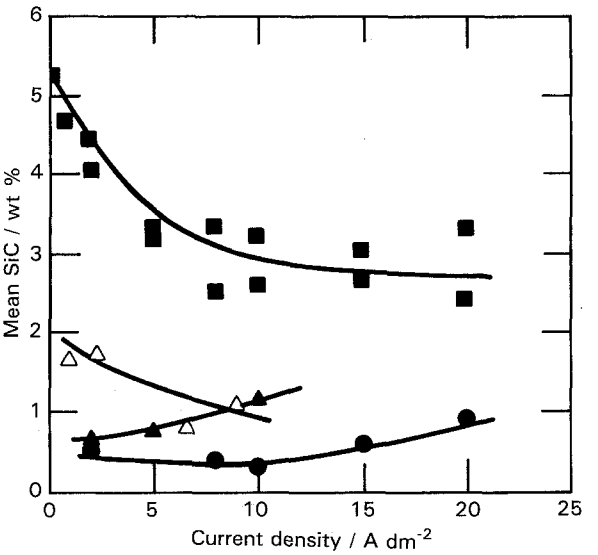

Fig. 11. Mean concentration of incorporated particles against current density for silicon carbide powders of various origins. ($C = 20\,g\,dm^{-3}$; $i = 10\,A\,dm^{-2}$; $\Omega = 500$ rpm). (■) Lonza UF 05; (●) Wolters; (△) Ibiden S; (▲) experimental results of Guglielmi [20].

plotting α_L against the reduced variable $r\Omega C^{-1}$ for the high velocity regime only (Fig. 8).

3.3. *Effects of the powder characteristics*

The percentage of SiC particles embedded in the nickel electrodeposit strongly depends on the particle size. For diameters smaller than approx. 5 μm, it was observed that the incorporation generally tends to increase with the mean diameter [43]. For example the radial distributions of a UF 15 SiC powder for several rotation velocities are presented on Fig. 9. These curves have to be compared with Fig. 6, which corresponds to a UF 10 powder with a larger grain size. Two results are emphasized: (i) the incorporated fraction of UF 15 is less than in the case of UF 10 (and even less than UF 05), and (ii) the critical velocity which corresponds to the transition between the low velocity regime and the high velocity regime is higher than 700 rpm, whereas it was about 400 rpm for a UF 10 SiC powder.

In the case of very fine SiC powders, such as UF 32, the local weight concentration was always very low (less than 0.7%), (close to the detection threshold of the EDX analysis technique), and was practically independent of r over the entire rotation rate range. This indicates that the critical rotation velocity, Ω_c, was never reached.

The mean fraction of incorporated SiC was also measured against the current density for four kinds of Lonza SiC powders (Fig. 10) at a 500 rpm rotation velocity 500 rpm. For the biggest particles (UF 05 and UF 10) α_w was very important and decreased with the current density. For smaller particles, (UF 15 and UF 32) α_w was smaller but tended to increase with increase in current density. It is worth noting that the α_w against i curve obtained at 300 rpm with a UF 05 powder (Fig. 4) is very similar to that obtained at 500 rpm with a UF 15 powder (Fig. 10). This suggests that the partition between the low velocity regime and the high velocity regime is a function of the particle size. The smaller the particle diameter, the higher the critical rotation velocity becomes.

A limited number of similar investigations were carried out with silicon carbide powders from other origins (Table 1). Some typical experimental data, plotted as α_w against i curves, are summarized in Fig. 11. For the sake of comparison, we also report on the same figure the results published by Guglielmi [20]. It appears that Guglielmi's data and the curve obtained with Wolters SiC belong to the low rotation velocity regime (as for Lonza UF 15 and UF 32

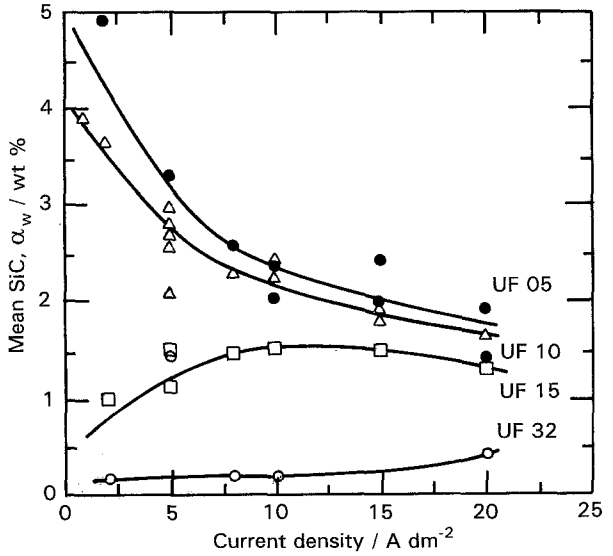

Fig. 10. Mean weight concentration of four kinds of Lonza SiC powders against current density. ($C = 20\,g\,dm^{-3}$; electrode diam: 20 mm, $\Omega = 500$ rpm). (●) UF 05, (△) UF 10, (□) UF 15 and (○) UF 32.

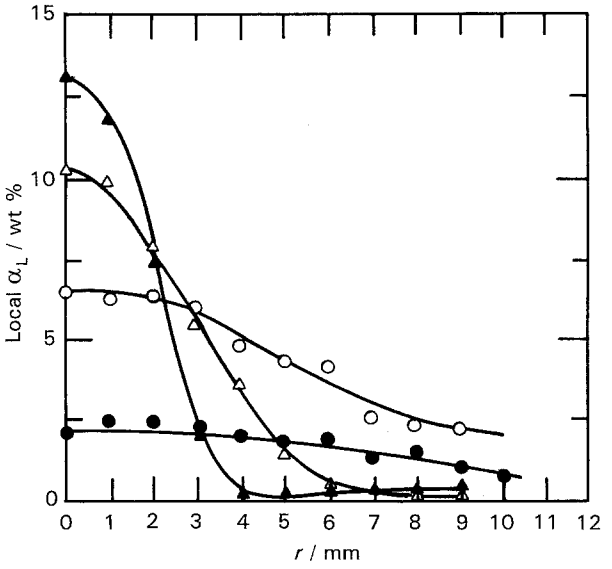

Fig. 12. Effect of xanthan gum on the radial distribution of the local concentration of UF 10 SiC. ($C = 20\,g\,dm^{-3}$, $i = 10\,A\,dm^{-2}$). Without additive: (●) $\Omega = 700$ rpm; with $1\,g\,dm^{-3}$ of Rhodopol^{TM}: (○) 300 rpm; (△) 700 rpm; (▲) 1500 rpm.

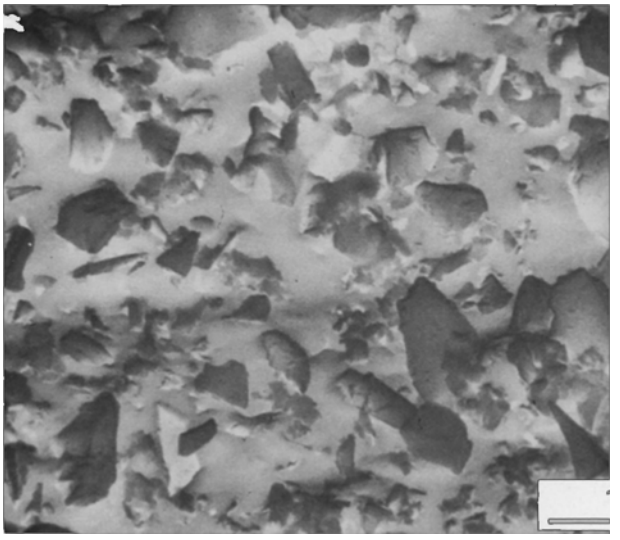

Fig. 13. SEM micrograph of the central part of Ni/SiC composite coating prepared in the presence of Rhodopol^{TM}. (UF 10 SiC: $C = 20\,g\,dm^{-3}$, $\Omega = 700$ rpm; $i = 10\,A\,dm^{-2}$).

powders on Fig. 9). Neither the characteristics of the SiC powder nor the stirring conditions used by Guglielmi are known. Nevertheless, it is worth noting that the incorporation fraction for the Wolters powder is very low, although their mean particle diameter is much larger (about 4 μm) than the Lonza powders. In the case of Ibiden-S powder, in spite of an even larger size (about 10 μm) the incorporated fraction is small. In this particular case, it is possible that the vertical motion of these very big particles toward the disc electrode is impeded by gravity. These comparative data suggest that the physico-chemical properties of SiC particles and, in particular, their surface composition also play a prominent role in the codeposition process.

3.4. *Influence of xanthan gum*

To avoid sedimentation of the particle suspension in the plating tank, Foissy and Desbois [44] proposed the incorporation of small quantities of a rheologic agent in a Ni/SiC composite coating plating bath. They used Rhodopol^{TM}, which is the commercial name of xantham gum produced by Rhone–Poulenc Company. This compound is made of long chain polysaccharid molecules; it is commonly used for stabilizing and thickening emulsions and suspensions. These authors found that this additive significantly increased the SiC content of the composite coating. A set of experiments was performed in a similar way as above after adding $1\,g\,dm^{-3}$ Rhodopol^{TM} in the plating bath. Rhodopol^{TM} has a spectacular effect: the mean concentration of incorporated SiC increased by a factor 2 for a 20 mm electrode and even more for smaller electrodes. In most of the experimental domain, the variations of α_w against i or against Ω became characteristic of the high velocity regime. Figure 12 shows how the radial distribution of SiC content is also strongly affected. Near the centre of the disc, the local SiC concentration may reach values as high as 13% by weight instead of about 4% in the absence of the additive. Conversely, away from the centre, the SiC concentration is dramatically diminished and may be lower than that without additive, especially for high rotation rates. It is worth noting that, in the presence of Rhodopol^{TM}, the radial distribution curves obtained with a very fine SiC powder (Lonza UF 32) [43] have the same form as those obtained with UF 10 (Fig. 12). In the central part of a composite coating prepared in the presence of Rhodopol^{TM} (Fig. 13) the concentration of attached particles is very high and, as mentioned above, most of the crystallites stand vertically. In addition, a very smooth nickel surface with the presence of cracks was observed on the SEM images. This shows that xanthan gum behaves as a brightening agent for nickel electrodeposition but the incorporation of organic species induces internal stresses in the nickel matrix which may affect the mechanical and the protective qualities of the coating.

4. Discussion and conclusion

Use of a rotating disc electrode, has shown that both steps of the nickel/particle codeposition process is affected by hydrodynamics in spite of the fact that this factor is not considered in the Guglielmi model [42, 43, 47]. For example, the apparent adsorption coefficient is very sensitive to bath agitation and depends on it in a complex way (Table 2).

Recently, Fransaer *et al.* [45, 46] derived a new codeposition model based on detailed analysis of particle trajectories by taking into account all particle–electrode interaction forces, as well as hydrodynamic forces. Particles are subjected to gravitational force, F_g, which, in our setup (Fig. 14(a)) was balanced by the vertical force, F_e, resulting from the liquid circula-

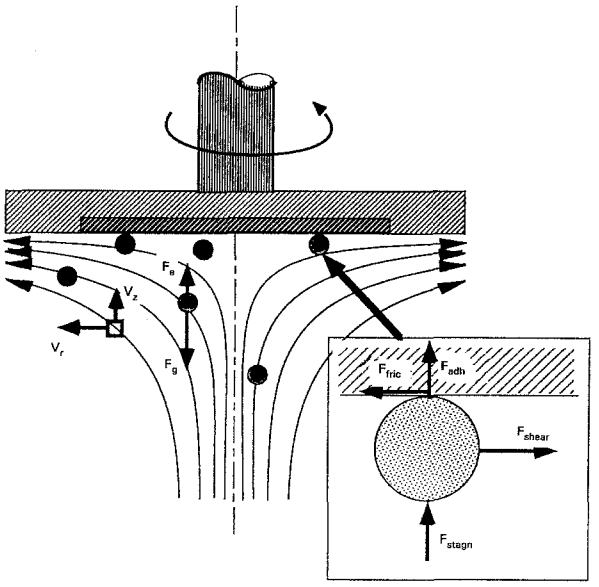

Fig. 14. Schematic diagram representing forces acting: (a) on particles approaching the rotating disc electrode. (b) on a particle attached to the surface (enlarged view).

tion by the external pumping circuit and to the forces exerted by the convective flow of the rotating disc electrode and, eventually, to attractive forces from the electrode surface if the particle approaches sufficiently close. For non-Brownian particles, the model shows that small particles tend to follow the fluid streamlines while the big particles tend to leave the streamlines when close to the wall. Particles which are attached to the surface are submitted to adhesion forces, F_{adh}, and frictional forces, F_{fric}, by the electrode surface and to a stagnation force, F_{stagn}, and a shear force, F_{shear}, by the fluid flow (Fig. 14(b)).

In the 'perfect sink' hypothesis, any colliding particle is permanently captured and a homogeneous radial distribution is therefore expected on a uniformly accessible electrode. This case corresponds to our experimental results obtained in the low velocity regime with a fine SiC powder below the critical rotation rate (Figs 6 and 9). Under these conditions, the concentration of entrapped SiC increases with the rotation rate. For bigger particles, and larger flow rates, i.e. in the high velocity regime, the perfect sink hypothesis no longer holds. It is necessary to take into account the effect of the shear force exerted by the fluid flow parallel to the wall on the attached particles, which tends to remove them before they become definitively entrapped in the metal layer. In the Fransaer model, a simple criterion was defined: an attached particle will be ejected if F_{shear} is larger than the sum of the adhesion force, F_{adh}, and the stagnation force, F_{stagn}, which both tend to maintain the particle in contact with the electrode. Thus, on a RDE one may expect a sudden drop of the incorporation rate as soon as the radial distance becomes larger than a critical value, r_c, where F_{shear} becomes greater than $(F_{shear} + F_{adh})$. In fact, F_{adh} has a distribution due to local surface physical imperfections and to the surface roughness. The size distribution of particles enhances this effect: only the small diameter fraction of the particulate can be captured at large radial distances. Finally, the α_L against r curve looks like a sigmoïd (Figs 6, 7 and 9). The mean quantity of incorporated SiC can be deduced by integrating this curve over the entire electrode radius. As such, the decrease in the mean quantity of embedded particles with the electrode radius can be understood (Fig. 5). The critical radius, which corresponds to a local fraction α_L equal to 50% of α_{max}, measured at the centre is a function of the particle diameter, the rotation rate, the fluid viscosity and the adhesion forces [47].

The adhesion forces are complex. In the low velocity range, the presence of a maximum in the α_w against i curves indicates that the probability of particle capture increases with cathodic polarization. For the Al_2O_3/Cu system it has been advanced that the adhesion force is maximum at the point of zero charge (PZC) of copper [46]. The strong influence of the potential on the particle codeposition rate observed in the case of very thin γ-Al_2O_3 powder with nickel [48] was ascribed to a field assisted attraction of the particles to the surface. But for high current densities, the particle codeposition rate was limited by mass transport, and maximum codeposition occurred at the current density corresponding to the transition between the two regimes. Moreover, the nickel deposition efficiency decreased because of the presence of attached particles. We did not observe similar perturbations of the nickel electrodeposition process, probably because the size of the SiC particles used was several orders of magnitude larger, and so, for a given quantity of matter, the interfacial double layer was much less affected. Recently Yeh and Wan [49] proved that the SiC surface is covered by a silica layer terminated by silanol groups with a PZC of 2.2. At pH > PZC, SiC particles adsorb nickel ions in the form of SiO^-Ni^{2+}, which can be reduced at the interface to a form of $SiONi_{ads}$ at a different rate than for Ni^{2+} or Ni^+_{ads}. The significant differences in incorporation rates observed in the present work with the various kinds of SiC powders (Fig. 11) seems to result mainly from the oxygen content of the particle surfaces (Table 1). In particular, the highest particle concentrations were obtained with Lonza powders, which exhibit the largest superficial oxygen content according to SIMS analysis. The crystal structure of silicon carbide may be another factor. The vertical position of SiC platelets (Fig. 13) may result from an anisotropy of superficial chemical bonds with respect to the crystal orientations of the various faces of the polyhedral particles.

Xanthan gum has a beneficial effect by maintaining particles in homogeneous suspension in the electrolyte volume but the strong augmentation of the mean concentration of incorporated SiC is mainly due to an increase in the electrolyte viscosity and, to a lower extent, to an increase in adhesion forces. The addition of $1\,g\,dm^{-3}$ of Rhodopol® to a nickel plating bath increases its kinematic viscosity by two orders of magnitude and the hydrodynamic forces applied on

attached particles are enhanced in the same proportion. As a consequence, the local SiC concentration can be increased by a factor of 3 at the center of the disc electrode, but conversely α_L decreases very rapidly with radial distance because of the strong ejection force, F_{shear}, especially at high rotation rates.

In conclusion, in spite of the recent work which strongly suggests that particle to electrode adhesion is potential assisted and also that the reduction of adsorbed cations is involved in the mechanism of SiC particle attachment, the Guglielmi model is unable to explain experimental results as soon as hydrodynamic conditions are modified. The present results are in full agreement with the Fransaer model which takes into consideration the effect of hydrodynamic forces on the approach and the ejection of particles. From a practical point of view, it appears necessary to control the hydrodynamic conditions to get a homogeneous and dense codeposit. In particular, it seems advantageous to maintain the fluid velocity gradient along the cathode at the level corresponding to the upper limit of the low velocity regime.

Acknowledgements

This work forms part of the doctoral thesis of Anne Lavanant and was made possible thanks to the financial support of the PSA (Peugeot–Citroën) company.

References

[1] R. Narayan and B. H. Narayana, *Coating Corros.* **4** (1981) 113,
[2] E. C. Kedward and B. Kiernam, *Metal Finish.* **13** (1967) 116.
[3] H. Hubner, O. Ostermann, *Galvanotechnik* **67** (1976) 452.
[4] C. E. Vest and D. F. Bazarre, *Metal Finish.* **45** (1967) 52.
[5] V. Sova and H. Bollhalder, Meeting of the Electrochem. Society, San Diego (1986), Abstract 709.
[6] H. Brown and T. Tomaszewski, Proceedings of 'Interfinish Surface 66', Forster Verlag, Zürich (1966) p. 88.
[7] S. Rashkov and N. Atanassov, *J. Appl. Electrochem.* **10** (1980) 535.
[8] F. K. Sautter, *J. Electrochem. Soc.* **110** (1963) 557.
[9] M. Verelst, J. P. Bonino and A. Rousset, *Mater. Sci. Engng* **A135** (1991) 51.
[10] E. S. Chen, G. R. Lakshinarayanan and F. K. Sautter, *Metall. Trans.* **2** (1971) 931.
[11] J. P. Celis and J. R. Roos, *J. Electrochem. Soc.* **124,** (1977) 1508.
[12] C. White and J. Foster, *Trans. Inst. Met. Finish.* **59** (1981) 8.
[13] C. C. Lee, C. C. Wan, *J. Electrochem. Soc.* **135** (1988) 1930.
[14] W. H. Safranek, 'The properties of electrodeposited metals and alloys', American Electroplaters Society Publications (1986).
[15] E. C. Edward, *Le Cobalt* (1973) p. 53.
[16] M. Thoma, *Plating Surf. Finish.* **71** (1984) 51.
[17] G. C. Pini, J. Weber, Proceedings of 'Interfinish 76', Amsterdam (1976), paper 41.
[18] C. Buelens, J. P. Celis and J. R. Roos, *J. Appl. Electrochem.* **13** (1983) 541.
[19] J. Zahavi and J. Hazan, *Plating Surf. Finish.* **2** (1983) 57.
[20] N. Guglielmi, *J. Electrochem. Soc.* **119** (1972) 1009.
[21] W. Metzer and T. Florian, *Metalloberfläche* **34** (1980) 274.
[22] Z. Zahavi and H. Kerbel, *Plating Surf. Finish.* (1982) 76.
[23] W. Metzer, R. Ott, G. Laux and H. Harst, *Galvanotechnik* **61** (1970) 998.
[24] V. P. Greco and W. Badauf, *Plating* (1968) 250.
[25] J. Foster and A. M. J. Kariapper, *Trans. Inst. Met. Finish.* **51** (1973) 27.
[26] M. Ruimi and R. Martinou, *Galvano-Organo Traitements de Surface* **595** (1989) 387.
[27] R. B. Narayan and R. N. Narayana, *J. Electrochem. Soc.* **128** (1981) 1704.
[28] R. Bazzard and P. J. Boden, *Trans. Inst. Met. Finish.* **50** (1972) 63.
[29] P. Pouderoux, J. P. Bonino and A. Rousset, Proceedings of 'Interfinish 92', Sao Polo (1992).
[30] C. Bhagwat, J. P. Celis and J. R. Roos, *Trans. Inst. Metal Finish.* **61** (1983) 72.
[31] M. Busson and M. Perinaud. Colloq. 'Innovations techniques dans le traitement de surface', Paris (1981).
[32] T. W. Tomaszewski, L. C. Tomaszewski and H. Brown, *Plating* **56** (1969) 1234.
[33] J. Zahavi and J. Hazan, Meeting of the Electrochemical Society, Montreal (1982), Abstract 690.
[34] P. W. Martin, *Metal Finish.* (1965) 399.
[35] C. Buelens, J. P. Celis and J. R. Roos, *Trans. Inst. Metal Finish.* **63** (1985) 6.
[36] J. P. Celis, J. R. Roos and C. Buelens, *J. Electrochem. Soc.* **134** (1987) 1402.
[37] C. Buelens, Doctoral Thesis, Katholieke Universiteit, Leuvan, Belgium (1984).
[38] A. M. J. Kariapper and J. Foster, *Trans. Inst. Met. Finish.* **52** (1974) 87.
[39] D. W. Snaith and P. D. Groves, *ibid.* **50** (1972) 95.
[40] J. Foster and B. Cameron, *ibid.* **54** (1976) 178.
[41] M. Ruimi, Thèse, Conservatoire National des Arts et Métiers, Paris (1987).
[42] A. Lavanant and G. Maurin, Meeting of the Electrochemical Society, Chicago, USA (1988), Abstract 343.
[43] A. Lavanant, Thèse de Doctorat de l'Université Pierre et Marie Curie, Paris, France (1991).
[44] N. Desbois, Thèse de Doctorat de l'Université de Franche Comté, Besançon, France (1992).
[45] J. Fransaer, J. P. Celis and J. R. Roos, *J. Electrochem. Soc.* **139** (1992) 413.
[46] J. Fransaer, Doctoral Thesis, Katholieke Universiteit, Leuven, Belgium (1994).
[47] G. Maurin and A. Lavanant, Meeting of the American Institute for Chemical Engineering, Miami Beach (1992), *in* Proceedings: 'Metal deposition and dissolution' (edited by D. T. Chin and R. E White), Electrochem. Society (1992) 107.
[48] P. Webb and N. Robertson, *J. Electrochem. Soc.* **141** (1994) 669.
[49] S. H. Yeh and C. C. Wan, *J. Appl. Electrochem.* **24** (1994) 993.